Temporal lenses for attosecond and femtosecond electron pulses

Shawn A. Hilbert[a], Cornelis Uiterwaal[a], Brett Barwick[b], Herman Batelaan[a], and Ahmed H. Zewail[b,1]

[a]Department of Physics and Astronomy, University of Nebraska-Lincoln, 116 Brace Laboratory, PO Box 880111, Lincoln, NE 68588-0111; and [b]Physical Biology Center for Ultrafast Science and Technology, Arthur Amos Noyes Laboratory of Chemical Physics, California Institute of Technology, Pasadena, CA 91125

Contributed by Ahmed H. Zewail, May 6, 2009 (sent for review April 17, 2009)

Here, we describe the ''temporal lens'' concept that can be used for the focus and magnification of ultrashort electron packets in the time domain. The temporal lenses are created by appropriately synthesizing optical pulses that interact with electrons through the ponderomotive force. With such an arrangement, a temporal lens equation with a form identical to that of conventional light optics is derived. The analog of ray diagrams, but for electrons, are constructed to help the visualization of the process of compressing electron packets. It is shown that such temporal lenses not only compensate for electron pulse broadening due to velocity dispersion but also allow compression of the packets to durations much shorter than their initial widths. With these capabilities, ultrafast electron diffraction and microscopy can be extended to new domains,and, just as importantly, electron pulses can be delivered directly on an ultrafast techniques target specimen.

attosecond imaging | ultrafast techniques

With electrons, progress has recently been made in imaging structural dynamics with ultrashort time resolution in both microscopy and diffraction (ref. 1 and references therein). Earlier, nuclear motions in chemical reactions were shown to be resolvable on the femtosecond (fs) time scale using pulses of laser light (ref. 2 and references therein), and the recent achievement of attosecond (as) light pulses (for recent reviews, see refs. 3–6) has opened up this temporal regime for possible mapping of electron dynamics. Electron pulses of femtosecond and attosecond duration, if achievable, are powerful tools in imaging. The ''electron recombination'' techniques used to generate such attosecond electron pulses require the probing electron to be created from the parent ions (to date no attosecond electron pulses have been delivered on an arbitrary target) and for general applications it is essential that the electron pulse be delivered directly to the specimen.

In ultrafast electron microscopy (UEM) (7), the electron packet duration is determined by the initiating laser pulse, the dispersion of the electron packet due to an initial energy spread and electron-electron interactions (see, e.g., ref. 8). Because packets with a single electron can be used to image (1, 7), and the initiating laser pulse can in principle be made very short ($<$10 fs), the limiting factor for the electron pulse duration is the initial energy spread. In photoelectron sources this spread is primarily due to the excess energy above the work function of the cathode (8), and is inherent to both traditional photocathode sources (9) and optically induced field emission sources (10–13). Energy-time uncertainty will also cause a measurable broadening of the electron energy spread, when the initiating laser pulse is decreased below $\approx$10 fs. For ultrafast imaging techniques to be advanced into the attosecond temporal regime, methods for dispersion compensation and new techniques to further compress electron pulses to the attosecond regime need to be developed.

A recent article by Baum and Zewail (14) has proposed a new technique for compressing free electron packets, from durations of hundreds of femtoseconds to tens of attoseconds, using spatially dependent ponderomotive potentials. The numerical results showed that a train of attosecond pulses can be created and used in ultrafast electron imaging. Because they are generated independent of the target they can be delivered to a specimen for studies of transient structures and electronic excitations on the attosecond time scale. In reference (14), the proposed compression concept was examined using numerical, electron trajectory calculations. The deflection of electrons [as in the Kapitza–Dirac effect (15)] by the ponderomotive potential of intense lasers (16) and the diffraction (17) of electrons in standing waves of laser light have been observed, and so is the possibility (described through computer modeling) of spatial/temporal focusing with combined time-dependent electric and static magnetic fields (18).

This article develops the ''temporal lens'' description that analytically expresses how ponderomotive compression can be used to both compensate for the dispersion and magnify (in this case compress) the temporal duration of electron packets. We obtain simple lens equations that have analogies in optics and the results of ''electron ray optics'' of temporal lenses reported here are entirely consistent with the findings of ref. 14, but now allow for analytical expressions and for the design of different schemes using geometrical optics. Here, we consider 2 types of temporal lenses: thin and thick.

For the realization of the temporal thin lens, a laser beam with a Laguerre–Gaussian transverse mode, radial index $\rho = 0$ and azimuthal index $l = 0$ [or, in common nomenclature, a ''donut'' mode (19–21)], is used. In the center of the donut mode, electrons will experience a spatially varying ponderomotive potential (intensity) that is approximately parabolic. This potential corresponds to a linear spatial force that, for chirped electron pulses, can lead to compression from hundreds of femtoseconds to $<$10 fs. The second type, that of a thick lens, which is the concept outlined in ref. 14, is based on the use of 2 counterpropagating laser beams to produce a spatially dependent standing wave that copropagates with the electrons. A train of ponderomotive potential wells are produced at the nodes of the standing wave, leading to compression but now with much ''tighter focus'' (thick lens). Because the electron copropagates with the laser fields the velocity mismatch is no longer a problem (14). Here, analytical expressions are derived showing that this lens has the potential to reach foci with attosecond duration, in agreement with the results of ref. 14. Finally, we discuss methods for creating tunable standing waves for attosecond pulse compression, and techniques for measuring the temporal durations of the compressed pulses. Space-charge dispersed packets of electrons that have a linear spatial velocity chirp (22, 23) may also be compressed with the temporal lenses described here.

Author contributions: S.A.H., C.U., B.B., H.B., and A.H.Z. designed research, performed research, contributed new reagents/analytic tools, analyzed data, and wrote the paper.

The authors declare no conflict of interest.

[1]To whom correspondence should be addressed. E-mail: zewail@caltech.edu.

This article contains supporting information online at www.pnas.org/cgi/content/full/0904912106/DCSupplemental.

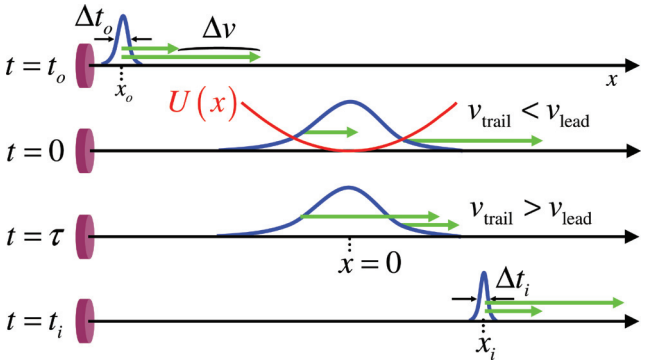

Fig. 1. Dispersion of an ultrashort electron packet. At $t = t_o$, the packet is created from a photocathode and travels with a velocity v_0. As it propagates along the x axis it disperses, with the faster electrons traveling further, and the slower ones trailing for a given propagation time t. At $t = 0$ a parabolic potential is pulsed on, giving an impulsive ''kick'' to the dispersed electron packet. After the potential is turned off, $t > \tau$, the trailing electrons now have a greater velocity than the leading electrons. After a propagation time $t = t_i$, the pulse is fully compressed.

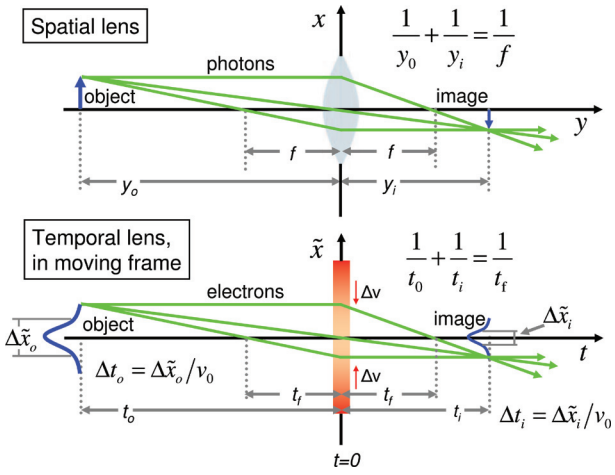

Fig. 2. Ray diagrams for spatial and temporal lenses. (*Upper*) Depicts 3 primary rays for an optical thin spatial lens. The object is located at y_o, and the spatial lens has a focal length, f. A real image of the object is created at the image plane, position y_i. (*Lower*) Ray diagram for a temporal thin lens. The diagram is drawn in a frame moving with the average speed v_0 of the electron packet. The slopes of the different rays in the temporal diagram correspond to different initial velocities that are present in the electron packet. As shown in the diagram a temporal image of the original electron packet is created at the image time t_i. The initial packet (object) is created at a time t_o with $\Delta t_o = \Delta x_o/v_0$, where the spatial extend of the pulse is directly related to the temporal duration of the object. The lens is pulsed on at $t = 0$ and the temporal focal length of the lens is t_f. The lens represents the ponderomotive potential and in this case is on for the very short time τ.

Results and Discussion

Preliminaries: Temporal Lens Concepts. All electron sources, both cw and pulsed, have an initial energy spread. For pulsed electron sources this is particularly relevant as electron packets created in a short time disperse as they propagate. The initial energy spread leads to an initial spread in velocities. These different velocities cause the initial packet to spread temporally, with the faster electrons traveling a further distance and the slower electrons traveling a shorter distance in a given amount of time. The dispersion leads to a correlation between position (along the propagation direction) and electron velocity (see Fig. 1). The linear spatial velocity "chirp" can be corrected for with a spatially dependent linear impulsive force (or a parabolic potential). Thus, if a pulsed, spatially dependent parabolic potential can be made to coincide appropriately with the dispersed electron packet, the slow trailing electrons can be sped up and the faster leading electrons can be slowed down. The trailing electrons, now traveling faster, can catch the leading electrons and the electron pulse will thus be compressed.

Consider a packet of electrons, propagating at a speed v_0 along the x axis, with a spread in positions of $\Delta x_o = v_0 \Delta t_o$, at time $t = t_o$; see Fig. 1. At $t = 0$, a potential of the form $U(x) = \frac{1}{2}Kx^2$ interacts with the electron packet for a duration τ in the lab frame. The waist, or spatial extent of the potential (temporal lens) is chosen to be w, whereas the duration τ is chosen such that it is short compared with w/v_0. When this condition is met the impulse approximation holds, and the change in velocity is $\Delta v = -\tau/m(dU(x)/dx) = -\tau Kx/m$, for $x < w$, where m is the electron mass. After the potential is turned off, $t > \tau$, the electrons will pass through the same position, $x_f - x = (v_0 + \Delta v)t_f$, at the focal time $t_f = -x/\Delta v = m/(K\tau)$. To include an initial velocity spread around v_0 (due to an initial ΔE), consider electrons that all emanate from a source located at a fixed position on the x axis. An electron traveling exactly at v_0 will take a time t_0 to reach the center of the potential well at $x = 0$. Electrons leaving the source with other velocities $v_0 + v_k$ will reach a location $x = v_k t_o$ at $t = 0$ (Fig. 2). The image is formed at a location where electrons traveling with a velocity v_0 and a velocity $v_0 + v_k$ intersect, this is, when $v_0 t_i = x + (v_0 + \Delta v + v_k)t_i$. The image time t_i is then $t_i = -x/(\Delta v + v_k)$.

For the object time, $t_o = x/v_k$, image time $t_i = -x/(\Delta v + v_k)$ and the focal time $t_f = -x/\Delta v$, the temporal lens equation holds,

$$\frac{1}{t_o} + \frac{1}{t_i} = \frac{1}{t_f} \qquad [1]$$

Ray tracing for optical lenses is often used to visualize how different ray paths form an image, and is also useful for visualizing how temporal lenses work, see Fig. 2. As derived in later sections the magnification M is defined as the ratio of the electron pulse duration (Δt_i) at the image position to the electron pulse duration (Δt_o), and is directly proportional to the ratio of the object and image times ($-t_i/t_o$) and distances ($-x_i/x_o$).

Femtosecond Thin Lens. In polar coordinates a Laguerre–Gaussian (LG_0^1) mode has a transverse intensity profile given by, $I(r,\varphi) = I_0 \exp(1) 2r^2 \exp(-2(r/w)^2)/w^2$ where w is the waist of the focus and I_0 the maximum intensity (19–21). This "donut" mode has an intensity maximum located at $r = \sqrt{2}|w|/2$ with a value of $I_0 = 2E_P\sqrt{\ln 2/\pi^3}/(w^2\tau)$ where E_P is the energy of the laser pulse and τ is the full-width-at-half-maximum of the pulse duration, assuming a Gaussian temporal profile given by $\exp(-4\ln 2(t/\tau)^2)$. The ponderomotive energy $U_P(x)$ is proportional to intensity (24),

$$U_p(x) = \frac{1}{2}\left[\frac{e^2\lambda^2 \exp(1) I_0}{2\pi^2 m \varepsilon_0 c^3 w^2}\sqrt{\frac{\ln 2}{\pi}}\right]x^2 \equiv \tfrac{1}{2}Kx^2, \qquad [2]$$

where m is the electron mass, e is the electron charge and λ the central wavelength of the laser radiation and replacing r with x. Near the center of the donut mode focus (or $x \ll w$) the intensity distribution is approximately parabolic, and hence the ponderomotive energy near the donut center is also parabolic. In analogy with a mechanical harmonic oscillator, the quantity in the square brackets of Eq. **2** can be referred to as the stiffness K; it has units of J/m^2 = N/m, and at 800 nm has the numerical value of, $K \approx 3.1 \times 10^{-36} E_P/(w^4\tau)$. For this parabolic approximation to be applicable, the spatial extent of the dispersed electron pulse, at

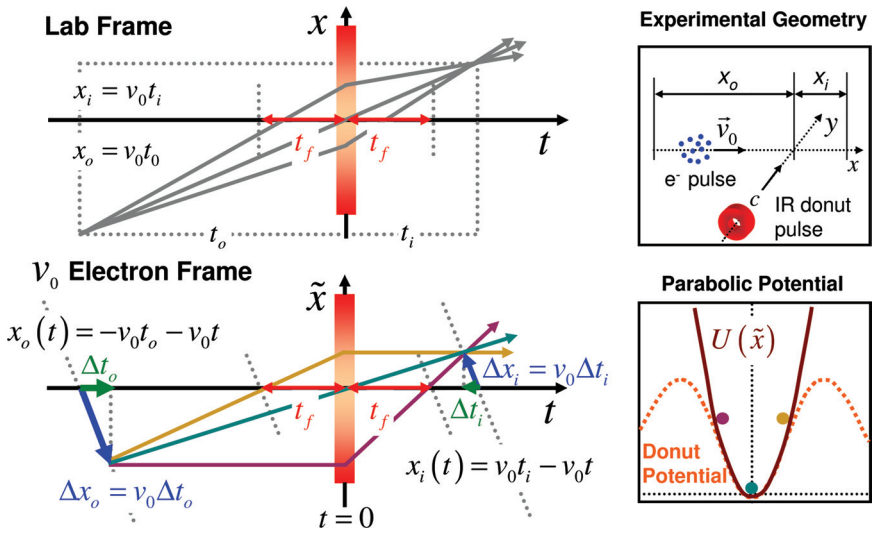

Fig. 3. Thin lens temporal ray diagrams for the lab and copropagating frames. (*Upper Left*) Ray diagram drawn in the lab frame showing how different initial velocities can be imaged to a single position/time. The gray lines are rays representing electrons with different velocities. (*Lower Left*) Ray diagram drawn in a frame moving with the average velocity v_0 of the electron packet. The rays represent velocities of $v_0/67$, $v_0/100$, and 0. In the copropagating frame, the relationship between Δt_o and Δt_i can be visualized as $\Delta t_i = -\Delta t_o t_i/t_o$. One major difference between the lab frame and the moving frame is that in the latter the position of the object and image are moving. The lines representing the object and the image positions are drawn with slopes of $-v_0$. (*Upper Right*) Experimental geometry for the implementation of a thin temporal lens. Note that the laser pulse and electron packet propagate perpendicular to each other, and that the interception point between the electrons and photons is at $x = 0$ and $t = 0$. (*Lower Right*) Shows how the parabolic (idealized) potential compares to the experimentally realizable donut potential. The colored dots indicate the position of electrons following the rays indicated in *Lower Left*.

$t = 0$, $\Delta x\,(0) = v_0 \Delta t_o + \Delta v_o t_o$ must be much smaller than the laser waist, where the object velocity spread is $\Delta v_o = \Delta E/\sqrt{2mE}$ (8).

The effect of this parabolic potential on an ensemble of electrons emitted from a source will now be analyzed (for detailed derivation, see *SI Appendix*). The velocity distribution of the ensemble is centered around v_0, with an emission time distribution centered on $-t_o$, where all electrons are emitted from the same location $x_o = -v_0 t_o$. Assuming a single donut-shaped laser pulse is applied at $t = 0$, and centered at $x = 0$, the electron ensemble is then influenced by the potential $U(x) = (1/2)Kx^2$. The k^{th} electron in the ensemble has an initial velocity $v_0 + v_k$ and emission time $-t_o + t_k$. Using a Galilean transformation to a frame moving with velocity v_0, the propagation coordinate x (lab frame) is replaced with the moving frame coordinate $\tilde{x} = x - v_0 t$. At $t = 0$ the potential exists for the ultrashort laser pulse duration τ, giving the electron an impulse (or 'kick') dependent on its instantaneous position in the parabolic potential. In both frames, the position of the electron at $t = 0$ is $x_k\,(0) = \tilde{x}_k\,(0) \equiv -v_0 t_k + v_k t_o - v_k t_k$, where $x_k(t)$ and $\tilde{x}_k(t)$ are in the lab and moving frames, respectively. Using the impulse approximation the electron trajectory immediately after the potential is turned off becomes,

$$\tilde{x}_k(t) = v_k t + \tilde{x}_k(0)(1 - t/t_f) \qquad [3]$$

where $t_f = m/(K\tau)$ is the focal time. The electron trajectories, before and after $t = 0$, can be plotted in both frames to give the equivalent of a ray diagram, Fig. 3. Electrons emitted at the same time, i.e., $t_k = 0$, but with different velocities, will meet at the image position, $\tilde{x}_k = 0$ in the moving frame at the image time t_i. The image time is found by setting $\tilde{x}_k(t_i) = 0$, from Eq. **3**, with $t_k = 0, \tilde{x}_k(t_i) = v_k t_i + v_k t_o(1 - t_i/t_f) = 0$, which is equivalent to the lens equation, Eq. **1**: $t_o^{-1} + t_i^{-1} = t_f^{-1}$.

An expression for the magnification can be obtained when electrons that are emitted at different times t_k and different velocities v_k are considered (see *SI Appendix* for detailed derivation). If the magnification is defined as $M = -t_i/t_o$ then the temporal duration at the image time becomes,

$$\Delta t_i = M \Delta t_0, \qquad [4]$$

where Δt_o and Δt_i are the duration of the electron packet at the object and image time, respectively. Durations achievable with a thin temporal lens follow from Eq. **4**.

An experimentally realistic temporal lens would use a 50-fs, 800-nm laser pulse with 350 μJ energy, focused to a waist of $w = 25$ μm. These values result in a stiffness of $K = 5.5 \times 10^{-8}$ N/m and a focal time of $t_f = 0.3$ ns; $t_f = m/(K\tau)$. If the lens is applied 10 cm from the source, electrons emitted at $v_0 = c/10$ (3 keV) would have an object time of $t_o = x_o/v_0 = 0.1/(c/10) = 3.0$ ns. Using the temporal lens equation, Eq. **1**, t_i is obtained to be 0.33 ns. Hence, a magnification of $M = -t_i/t_o = 0.1$. Consequently, a thin temporal lens can compress an electron packet with an initial temporal duration of $\Delta t_o \approx 100$ fs, after it has dispersed, to an image duration of $\Delta t_i \approx 10$ fs. Although the example presented here is for 3 keV electrons, the thin lens approximation holds for higher energy electrons as long as τ is chosen to be short compared with w/v_0. Experimentally, the thin temporal lens can be used in ultrafast diffraction experiments (25), which operate at kHz repetition rates with lasers that typically possess power that exceeds the value needed for the ponderomotive compression.

Attosecond Thick Lens. In the previous section it was analytically shown that free electron packets can be compressed from hundreds to tens of femtoseconds using a temporal thin lens, which would correspond to a magnification of ≈ 0.1. However, the analytic solutions used rely on an impulse approximation that may not generally hold for the temporal lens described in ref. 14. For example, ref. 14 numerically showed that a $\approx$300-fs duration electron packet can be compressed to a train of $\approx$15 as pulses, which corresponds to a magnification of $M \approx 5 \times 10^{-5}$; the associated image time of $t_i = 2$ ps is comparable with the laser pulse duration of $\tau = 0.3$ ps. Because $M \ll 1$ and t_i and τ are the same order, it is unclear whether the impulse approximation would accurately describe the results.

Another issue that needs to be addressed is how an initial

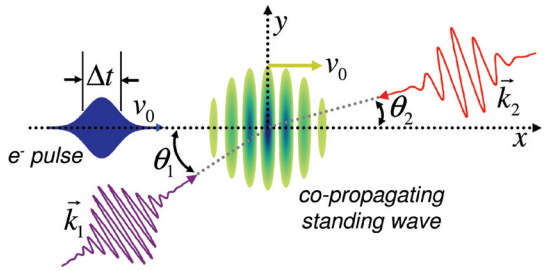

Fig. 4. 2D schematic of tilted laser pulse concept for copropagating standing wave used for attosecond electron compression (thick temporal lens). When $\theta_1 = \theta_2 = 0$, then $v_0 = c/3$ for ω and 2ω beams (14). With frequencies of ω and 2ω the velocity of the copropagating standing wave can be tuned by tilting the 2 laser pulses angles θ_1 and θ_2. When the 2 angles are chosen according to $\theta_2 = \arcsin(2\sin\theta_1)$, the wells in the standing wave are perpendicular to the electron propagation.

source velocity spread and dispersion affects the ability for the temporal lens in ref. 14 to compress electron packets. The simulation done in ref. 14 predicted ≈15 as electron pulses, where the duration was determined solely by the sinusoidal deviation from the optimal parabolic potential, and did not allow the electron packet to disperse before compression. In the thin lens case, an initial velocity spread results in a nonzero pulse duration even with a parabolic potential. Developing a model incorporating an electron packet that is allowed to disperse before encountering a parabolic potential will answer whether or not an initial velocity spread is detrimental to attosecond pulse compression.

The attosecond compression scheme presented in ref. 14 relies on the presence of a standing wave that copropagates with an ultrashort electron pulse. The copropagating standing wave is created by using 2 different optical frequencies, constructed by having a higher frequency (ω_1) optical pulse traveling in the same direction as the electron packet and a lower frequency (ω_2) traveling in the opposite direction. When the optical frequencies ω_1, ω_2, and the electron velocity v_0 are chosen according to $v_0 = c(\omega_1 - \omega_2)/(\omega_1 + \omega_2)$, a standing wave is produced in the rest frame of the electron (14) (see Fig. 4). If the electron has a velocity $v_0 = c/3$, and $\omega_1 = 2\omega_2$ then the copropagating standing wave has a ponderomotive potential of the form (24),

$$U_p(x) = \frac{1}{2}\left(\frac{e^2\tilde{\lambda}^2E_0^2}{8\pi^2mc^2}\right)\cos^2(\tilde{k}x), \qquad [5]$$

where E_0 is the peak electric field, $\tilde{\lambda}$ the Doppler shifted wavelength (14). The envelopes of the laser pulses are ignored in this derivation, but they can be engineered so that the standing wave contrast is optimized (26).

To find an analytic solution in the thick lens geometry, each individual potential well in the standing wave is approximated by a parabolic potential that matches the curvature of the sinusoidal potential, $U_P(x) = (1/2)[e^2E_0^2/(2mc^2)]x^2 \equiv (1/2)Kx^2$. Using the exact solution to the harmonic oscillator the focal time is,

$$t_f = \cot(\omega_p\tau)/\omega_p + \tau, \qquad [6]$$

where $\omega_p = \sqrt{Km}$ and τ is the duration that the lens is on. For $\tau \to 0$, $t_f \to m/(K\tau)$, which is identical to the thin lens definition. The image time, t_i, has a form,

$$t_i = (1/\omega_p^2 + t_0t_f - t_f\tau + \tau^2)/(t_0 - t_f + \tau), \qquad [7]$$

and after the 2 assumptions, $\tau \to 0$ and $t_o \gg 1/(t_f\omega_p^2)$ becomes equivalent to Eq. **1**, the lens equation: $t_o^{-1} + t_i^{-1} = t_f^{-1}$.

The standard deviation of the compressed electron pulse at arbitrary time t_a is,

$$\Delta t_a = \sqrt{\frac{t_f^2(\tilde{\lambda}^2 + 4t_a^2\Delta v_o^2) + t_a^2\tilde{\lambda}^2 - 2t_ft_a\tilde{\lambda}^2}{48t_f^2v_0^2}}, \qquad [8]$$

which is valid for an individual well (detailed derivation in the *SI Appendix*). The time when the minimum pulse duration occurs is $t_a = t_f\tilde{\lambda}^2/(\tilde{\lambda}^2+4t_f^2\Delta v_o^2) \approx t_f$ and for experimentally realistic parameters is equal to t_f. This implies that the thick lens does not image the initial temporal pulse; it temporally focuses the electrons that enter each individual well. Because there is no image in the thick lens regime, the minimum temporal duration is not determined by the magnification M as in the thin lens section, but is a given by,

$$\Delta t_f = \sqrt{\frac{t_f^2\tilde{\lambda}^2\Delta v_o^2}{12v_0^2(\tilde{\lambda}^2 + 4t_f^2\Delta v_o^2)}} \cong \frac{t_f\Delta v_o}{v_0^2 2\sqrt{3}}, \qquad [9]$$

which is equivalent to Eq. **6** in ref. 14. It should be noted that neither the temporal focal length nor the temporal duration are directly dependent on the Doppler shifted wavelength $\tilde{\lambda}$, as long as the condition $t_o < v_0\Delta t_o/\Delta v_o$ is met.

An example illustrates what temporal foci are obtainable. A source emits electrons with an energy distribution of 1 eV and a temporal distribution of 100 fs. Electrons traveling at $v_0 = c/3$ and having an energy $E = 31$ keV gives a velocity distribution of $\Delta v_o = 1670$ m/s. If the distance between the source and the temporal lens is 10 cm, $t_o = 1.0$ ns is less than $v_0\Delta t_o/\Delta v_o \approx 6.0$ ns, satisfying the condition $t_o < v_0\Delta t_o/\Delta v_o$ and Eq. **9** is then valid. If the 2 colors used for the laser beams are 520 nm and 1040 nm, the Doppler-shifted wavelength is $\tilde{\lambda} = 740$ nm. For a laser intensity of 3×10^{12} Wcm^{-2} (available with repetition rates up to megahertz), the oscillation frequency in the potential well is $\omega_p \approx 2 \times 10^{12}$ rad/s, which gives a focal time of $t_f \approx 1$ ps. With these parameters, Eq. **9** gives a temporal duration at the focus of $\Delta t_f \approx 5$ as. To support this ≈5 as electron pulse, time-energy uncertainty demands an energy spread of ≈50 eV. The ponderomotive compression imparts an energy spread to the electron pulse, which can be estimated from $\Delta E \approx mv_0\tilde{\lambda}(2t_f)$, giving ≈50 eV similar to the uncertainty limit. This ΔE is very small relative to the accelerating voltage in microscopy (200 keV) and only contributes to a decrease of the temporal coherence. In optical spectroscopy such pulses can still be used as attosecond probes despite the relatively large ΔE when the chirp is well characterized (27). Combining the anharmonicity broadening of 15 as (as discussed in ref. 14), we conclude that ultimately temporal pulse durations in the attosecond regime can be reached.

Tunable Thick Lens. In the temporal thick lens case, the use of ω and 2ω to create a copropagating standing wave requires $v_0 = c/3$. However, the velocity of the electrons, v_0, can be tuned by changing the angle of the 2 laser pulses. A copropagating standing wave can still be obtained by forcing the Doppler-shifted frequencies of both tilted laser pulses to be equal. A laser pulse that propagates at an angle θ with the respect to the electron propagation direction has a Doppler-shifted frequency $\tilde{\omega} = \gamma\omega(1 \pm (v/c)\cos\theta)$, where ω is the angular frequency in the lab frame, $\vec{v} = v\hat{x}$ is the electron velocity, and $\gamma = 1/\sqrt{1 - v^2/c^2}$ (28). When the 2 laser pulses are directed as shown in Fig. 4, a copropagating standing wave occurs for an electron with a velocity $v_0 = c(k_1 - k_2)/(k_1\cos\theta_1 + k_2\cos\theta_2)$, where the laser pulse traveling with the electron packet has a wave vector of magnitude k_1 and makes an angle of θ_1 with the electron propagation axis; the second laser pulse traveling against has a wave vector magnitude of k_2 and angle θ_2, in the lab frame. An

electron moving at v_0 will see a standing wave with an angular frequency,

$$\tilde{\omega} = \frac{2(\cos\theta_1 + \cos\theta_2)}{2\cos\theta_1 + \cos\theta_2}\,\gamma\omega(1-\beta), \qquad [10]$$

where $2k = k_1 = 2k_2$ for experimental convenience, $\omega = kc$, and the wavelength is $\tilde{\lambda} = 2\pi c/\tilde{\lambda} = 2\pi/\tilde{\lambda}$.

The standing wave created with arbitrary angles θ_1 and θ_2 will be tilted with respect to the electron propagation direction, which will temporally smear the electron pulse. This tilting of the standing wave can be corrected for by constraining the angles θ_1 and θ_2 to be: $\theta_2 = \arcsin(2\sin\theta_1)$.

For $\theta_1 = 15^0$ (forcing $\theta_2 \approx 31^0$), electrons with velocity $v_0 = 0.36c$ ($E \approx 33$ keV) see a standing wave. A 1 eV electron energy distribution at the source gives a velocity distribution of $\Delta v_0 \approx 1630$ m/s, at 33 keV. Using the same laser intensity as in the thick lens case, and the new v_0 and Δv_o, the condition $t_o < v_0 \Delta t_o/\Delta v_o$ is still satisfied, allowing Eq. **10** to be used, resulting in a duration at the focus of $\Delta t_f \approx 4.6$ as. Using the tunable thick lens makes the experimental realization more practical, allowing for easy optical access and electron energy tuning, while at the same time keeping Δt_f approximately the same. For additional tunability, an optical parametric amplifier can be used so that the laser pulse frequencies are not restricted to ω and 2ω.

Detection Proposals. The ability to create electron pulses with duration from ≈10 fs to ≈10 as raises a challenge regarding the measuring of their duration and shape. Two different schemes are presented here for measuring pulses compressed by thick and thin temporal lenses. For measuring the thin lens compressed electron packet, the focused packet could be intersected by a laser pulse with a Gaussian spatial focus (Fig. 5). An optical delay line would control the time delay between the measuring laser pulse and the compressed electron packet. As the time delay, Δt, is varied, so is the average energy of the electrons, as shown in Fig. 5. If the delay time is zero, then the average electron energy will be unaffected, because there is no force. If the delay line is changed so that the Gaussian pulse arrives early (late), then the average energy will decrease (increase). The change in the average energy depends on the duration of the electron pulse, and the intensity of the probing laser pulse. If the electron pulse is longer than the duration of the measuring laser pulse, then the change in the average energy will be reduced. The steepness of the average energy as a function of delay time, $\bar{E}(\Delta t)$, is a direct measure of the electron pulse duration, and by using femtosecond-pulsed electron energy loss spectra (29) this scheme can be realized.

For the thick lens a similar method was proposed in ref. 14 and described in more detail here. At the focal position and time of the compressed temporal electron packet, a second copropagating potential is introduced. The positions of the individual wells in the second copropagating standing wave can be moved by phase shifting one of the two laser beams that create the probing potential (Fig. 5). By varying the phase shift, the potential slope (and hence the force) that the electrons encounter at the focus is changed. If no phase shift is given to the probing standing wave, no average energy shift results. When a phase shift is introduced, the electrons will be accelerated (or decelerated) by the slope of an individual well in the standing wave, and as long as the phase stability between the electrons and the probing standing wave is appropriate, attosecond resolution can be achieved. As the electron pulse duration becomes less than the period of the standing wave, the average electron energy change increases. The electron temporal duration of the compressed electron packet can be determined directly by the steepness of the $\bar{E}(\varphi)$ curve.

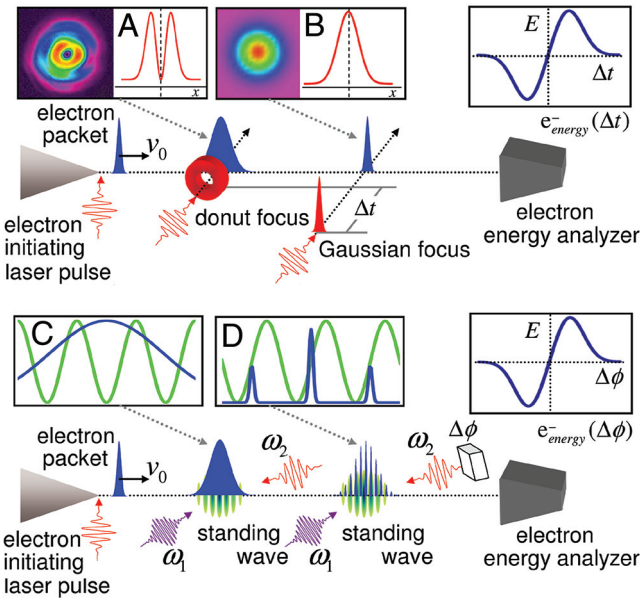

Fig. 5. Detection schemes for measuring femtosecond and attosecond compressed electron packets. (*Upper*) Depicts how femtosecond electron packets can be measured by intersecting the packet at the image position/time. (*A*) Spatial profile of the donut mode temporal lens. (*B*) Gaussian profile of the measuring laser pulse. As the time delay, Δt, between the measuring Gaussian laser pulse and the electron packet is varied the average energy of the electron pulse changes. (*Lower*) depicts the scheme for measuring the duration of attosecond pulses. (*C*) The spatial profile of the temporal lens at $t = 0$ is shown (green). (*D*) The second standing wave that is used to measure the pulse duration of the attosecond electron packets at $t = t_f$ is displayed. The blue lines in *C* and *D* give the spatial distribution of the electron packets at $t = 0$ and $t = t_f$, respectively. To measure the duration of the attosecond pulses, a second copropagating standing wave is made to coincide with the electron pulse at the focal position. Instead of using a temporal delay a phase shift, $\Delta\varphi$, is introduced into one of the laser pulses that creates the probing standing wave. By varying this phase shift the nodes of the standing wave shift position. The average electron energy can thus be plotted versus this phase shift. As the electron pulses become shorter than the period of the standing wave the change in the average energy will increase.

Conclusion and Outlook. The attosecond electron imaging regime is possible only when the electron pulses are compressed to the attosecond duration. Current efforts in employing attosecond technologies (primarily electron recombination) require the target specimen to be part of the electron generation, causing the pump and the probe to be coupled. Here, we have described 2 temporal lens designs and obtained analytical expressions consistent with the proposal of Baum and Zewail (14). With a thin temporal lens, the capability to image an electron packet temporally is illustrated with compressibility (or magnification) of the pulse duration from 100 fs to 10 fs. A thick temporal lens can focus an initial dispersed electron packet (hundreds of femtoseconds) into a train of attosecond pulses; this case is discussed in ref. 14 using electron trajectory simulations.

The ultrashort pulses produced by the temporal lenses described here, or by using other compression schemes (18, 30, 31), will have a wide range of applications in UEM (1, 7) and femtosecond-pulsed electron energy loss spectroscopy (29). Although single electron packets develop a linear velocity chirp due to dispersion, packets with linear chirp can be imaged with the temporal lenses described in this article. For an initial packet with an ellipsoidal distribution of electrons, electron-electron interactions (space charge) result in a linear spatial chirp in the propagation direction (23). This linear chirp due to space charge can be used to increase the temporal resolution of ultrafast

electron diffraction experiments through energy filtering (22) or pulse compression with radio-frequency fields (32). In principle, the concepts presented here can also be used to compress space-charge dominated pulses of electrons extending the range of applicability for temporal lenses.

Finally, temporal lenses have the potential to increase by orders of magnitude the quantum degeneracy of an electron packet (33). The first use of electron quantum degeneracy in free space—the demonstration of the Hanbury Brown and Twiss effect for electrons (antibunching)–reached a degeneracy value of 10^{-4} (34, 35) and in other sources could be 10^{-6} or less. This was done with a continuous electron beam from a field emission tip (34). By using pulsed sources and temporal lenses the degeneracy factor can become significantly closer to the quantum limit of one because of the increased current density during the pulse duration. In this limit, the potential for "electron quantum optics" becomes real.

ACKNOWLEDGMENTS. We thank Sang Tae Park for helpful discussions; Peter Baum for careful reading of the manuscript; and the 3 referees, Profs. F. Krausz, P. Corkum, and A. Bandrauk, for helpful comments. This work was supported by the National Science Foundation and the Air Force Office of Scientific Research in the Gordon and Betty Moore Center for Physical Biology at Caltech.

1. Zewail AH (2006) 4D ultrafast electron diffraction, crystallography, and microscopy. *Annu Rev Phys Chem* 57:65–103.
2. Zewail AH (2000) Femtochemistry: Atomic-scale dynamics of the chemical bond. *J Phys Chem A* 104:5660–5694.
3. Krausz F, Ivanov M (2009) Attosecond physics. *Rev Mod Phys* 81:163–234.
4. Corkum PB, Krausz F (2007) Attosecond science. *Nat Phys* 3:381–387.
5. Agostini P, DiMauro LF (2004) The physics of attosecond light pulses. *Rep Prog Phys* 67:813–855.
6. Kapteyn H, Cohen O, Christov I, Murnane M (2007) Harnessing attosecond science in the quest for coherent x-rays. *Science* 317:775–778.
7. Barwick B, Park HS, Kwon O-H, Baskin JS, Zewail AH (2008) 4D imaging of transient structures and morphologies in ultrafast electron microscopy. *Science* 322:1227–1231, and references therein.
8. Gahlmann A, Park ST, Zewail AH (2008) Ultrashort electron pulses for diffraction, crystallography and microscopy: Theoretical and experimental resolutions. *Phys Chem Chem Phys* 10:2894–2909.
9. Janzen A, et al. (2007) A pulsed electron gun for ultrafast electron diffraction at surfaces. *Rev Sci Instrum* 78:013906.
10. Hommelhoff P, Sortais Y, Aghajani-Talesh A, Kasevich M (2006) Field emission tip as a nanometer source of free electron femtosecond pulses. *Phys Rev Lett* 96:077401.
11. Ropers C, Solli DR, Schulz CP, Lienau C, Elsaesser T (2007) Localized multiphoton emission of femtosecond electron pulses from metal nanotips. *Phys Rev Lett* 98:043907.
12. Barwick B, et al. (2007) Laser-induced ultrafast electron emission from a field emission tip. *New J Phys* 9:142.
13. Gault B, et al. (2007) Optical and thermal processes involved in ultrafast laser pulse interaction with a field emitter. *Ultramicroscopy* 107:713–719.
14. Baum P, Zewail AH (2007) Attosecond electron pulses for 4D diffraction and microscopy. *Proc Natl Acad Sci USA* 104:18409–18414.
15. Kapitza PL, Dirac PAM (1933) The reflection of electrons from standing light waves. *Proc Cambridge Philos Soc* 29:297–300.
16. Bucksbaum PH, Schumacher DW, Bashkansky M (1988) High-intensity Kapitza–Dirac effect. *Phys Rev Lett* 61:1182–1185.
17. Freimund DL, Aflatooni K, Batelaan H (2001) Observation of the Kapitza–Dirac effect. *Nature* 413:142–143.
18. Monastyrskiy MA, et al. (2005) High-Speed Photography and Photonics. In *Proceedings International Society for Optical Engineering Vol 5580*, eds Paisley DL, Kleinfelder S, Snyder DR, Thompson BJ (SPIE, Bellingham, WA), pp 324–334.
19. Mariyenko IG, Strohaber J, Uiterwaal CJGJ (2005) Creation of optical vortices in femtosecond pulses. *Opt Express* 13:7599–7608.
20. Strohaber J, Petersen C, Uiterwaal CJGJ (2007) Efficient angular dispersion compensation in holographic generation of intense ultrashort paraxial beam modes. *Opt Lett* 32:2387–2389.
21. Kuga T, Torii Y, Shiokawa N, Hirano T (1997) Novel optical trap of atoms with a doughnut beam. *Phys Rev Lett* 78:4713–4716.
22. Baum P, Zewail A (2008) Femtosecond diffraction with chirped electron pulses. *Chem Phys Lett* 462:14–17.
23. Luiten OJ, van der Geer SB, de Loos MJ, Kiewiet FB, van der Wiel MJ (2004) How to realize uniform three-dimensional ellipsoidal electron bunches. *Phys Rev Lett* 93:094802.
24. Batelaan H (2007) Illuminating the Kapitza–Dirac effect with electron matter optics. *Rev Mod Phys* 79:929–941.
25. Baum P, Yang D-S, Zewail AH (2007) 4D visualization of transitional structures in phase transformations by electron diffraction. *Science* 318:788–792.
26. Imeshev G, Fejer MM, Galvanauskas A, Harter D (2001) Generation of dual-wavelength pulse by frequency doubling with quasi-phase-matching gratings. *Opt Lett* 26:268–270.
27. Yudin GL, Bandrauk AD, Corkum PB (2006) Chirped attosecond photoelectron spectroscopy. *Phys Rev Lett* 96:063002.
28. Jackson JD (1999) *Classical Electrodynamics* (John Wiley & Sons, Inc., New York), 3rd Ed.
29. Carbone F, et al. (2008) EELS femtosecond resolved in 4D ultrafast electron microscopy. *Chem Phys Lett* 468:107–111.
30. Fill E, Veisz L, Apolonski A, Krausz F (2006) Sub-fs electron pulses for ultrafast electron diffraction. *New J Phys* 8:272.
31. Veisz L, et al. (2007) Hybrid dc-ac electron gun for fs-electron pulse generation. *New J Phys* 9:451.
32. van Oudheuseden T, et al. (2007) Electron source concept for single-shot sub-100 fs electron diffraction in the 100 keV range. *J Appl Phys* 102:093501.
33. Spence JCH, Qian W, Silverman MP (1994) Electron source brightness and degeneracy from Fresnel fringes in field emission point projection microscopy. *J Vac Sci Technol A* 12:542–547.
34. Kiesel H, Renz A, Hasselbach F (2002) Observation of Hanbury Brown-Twiss anticorrelations for free electrons. *Nature* 418:392–394.
35. Spence JCH (2002) Quantum physics—Spaced-out electrons. *Nature* 418:377–378.